

CERTIFICATE

It is certified that the work contained in the thesis titled “**Studies on Al-Cu-Fe Quasicrystalline and 6082 Al-alloy based Metal Matrix Composites**” by “**YAGNESH SHADANGI**” has been carried out under our joint supervision and that this work has not been submitted elsewhere for a degree.

It is further certified that the student has fulfilled all the requirements of Comprehensive, Candidacy and SOTA for the award of Ph.D. degree.



Prof. N K Mukhopadhyay

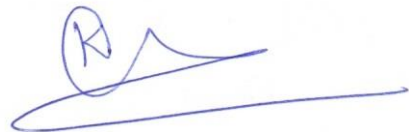
(Supervisor)

Professor in Physical Metallurgy

Department of Metallurgical Engineering

Indian Institute of Technology (BHU), Varanasi

Varanasi - 221005, Uttar Pradesh, India



Dr. Kausik Chattopadhyay

(Co-supervisor)

Associate Professor

Department of Metallurgical Engineering

Indian Institute of Technology (BHU), Varanasi

Varanasi - 221005, Uttar Pradesh, India

DECLARATION BY THE CANDIDATE

I, **YAGNESH SHADANGI**, certify that the work embodied in this Ph.D. thesis is my own bonafide work carried out by me under the joint supervision of **Prof. NILAY KRISHNA MUKHOPADHYAY** and **Dr. KAUSIK CHATTOPADHYAY** for a period from **JULY 2014** to **DECEMBER 2020** at the “**DEPARTMENT of METALLURGICAL ENGINEERING**”, Indian Institute of Technology (BHU), Varanasi. The matter embodied in this Ph.D. thesis has not been submitted for the award of any other degree/diploma. I declare that I have faithfully acknowledged and given credits to the research workers wherever their works have been cited in my work in this thesis. I further declare that I have not wilfully copied any other's work, paragraphs, text, data, results, *etc.*, reported in journals, books, magazines, reports dissertations, thesis, *etc.*, or available at websites and have not included them in this thesis and have not cited as my own work.

Date: December 30, 2020

Place: Varanasi



(YAGNESH SHADANGI)

CERTIFICATE BY THE SUPERVISOR

This is to certify that the above statement made by the candidate is correct to the best of our knowledge.



Prof. N K Mukhopadhyay

(Supervisor)

Professor in Physical Metallurgy

Department of Metallurgical Engineering

Indian Institute of Technology (BHU), Varanasi

Varanasi - 221005, Uttar Pradesh, India



Dr. Kausik Chattopadhyay

(Co-supervisor)

Associate Professor

Department of Metallurgical Engineering

Indian Institute of Technology (BHU), Varanasi

Varanasi - 221005, Uttar Pradesh, India

Forwarded by:



(Prof. Nilay Krishna Mukhopadhyay)

Head of Department

Department of Metallurgical Engineering

Indian Institute of Technology

(Banaras Hindu University)

Varanasi - 221005, India

COPYRIGHT TRANSFER CERTIFICATE

Title of the Thesis: Studies on Al-Cu-Fe Quasicrystalline and 6082 Al-alloy based Metal Matrix Composites

Candidate's Name: Yagnesh Shadangi

Copyright Transfer

The undersigned hereby assigns to the Indian Institute of Technology (Banaras Hindu University), Varanasi all rights under copyright that may exist in and for the above thesis submitted for the award of the *Doctor of Philosophy*.

Date: December 30, 2020

Place: Varanasi



(YAGNESH SHADANGI)

Note: However, the author may reproduce or authorize others to reproduce materials extracted verbatim from the thesis or derivative of the thesis for author's personal use provided that the source and the Institute's copyright notice are indicated.

ACKNOWLEDGEMENT

Before I start, I would like to thank, the almighty for guiding me through the years of my studies and giving me all strength required to sustain the days of hardship. I also bow in gratitude to almighty to have given me an opportunity to study in the Indian Institute of Technology (Banaras Hindu University) founded by visionary legend Mahamana Pandit Madan Mohan Malviya.

I will take this opportunity to express my sincere thanks and gratitude to my supervisors Prof. Nilay Krishna Mukhopadhyay and Dr. Kausik Chattopadhyay for their consistent guidance and encouragement during the entire duration of Ph.D. work. Their immense support has helped to sail through difficult situations encountered in last six years. There is saying that a great teacher always inspires students, for all his inspiration, I will be always thankful to Prof. N K Mukhopadhyay.

Besides my advisors, I would like to thank the rest of my RPEC members: Prof. Pralay Maiti (SMST) and Dr. Rampada Manna for their support and insightful comments. I would like to convey my sincere thanks to Prof. N K Mukhopadhyay (Head, Department of Metallurgical Engineering, IIT (BHU), Varanasi), Prof. R K Mandal and Prof. G.V.S. Sastry (Former Heads, Department of Metallurgical Engineering, IIT (BHU)) for their valuable comments, suggestions and needful help extended for conducting my research work. I will like to acknowledge Prof. R K Mandal (Co-ordinator, MSD, Dept. of Metallurgical Engg., IIT (BHU)) for his immense support through all these years. His timely suggestions and corrections has always helped me to improve. I will also like to thank Dr. Joysurya Basu for introducing and training me for operating TEM as an independent user. His mentorship has helped me to learn practical aspects of TEM.

I would like to extend my gratitude to Prof. Vakil Singh, Prof. S N Ojha and Prof. A K Ghose for inspiring me pursue my carrier in the field of research during my days as a post-graduate student of this department. I express my sincere thanks to entire faculty members of the department for their valuable suggestions. I will acknowledge Dr R Manna (Coordinator, ARCIS) and Prof. Rajiv Prakash (CIF, IIT (BHU)) for extending necessary characterization facility. I will like to express my gratitude to Dr. Bhaskar Majumdar (DIAT, Pune), Prof. K G Prashanth (TalTech, Estonia) and Dr V. Balakrishnan (IIT Mandi) for extending their help for SPS and nanoindentation studies.

My sincere thanks to Mr. Lalit Kumar Singh for his invaluable help extended during TEM investigation. I will also like to acknowledge Mr. Girish Sahu and Mr. Vinay (CIF, IIT (BHU)) for their constant help in conducting SEM studies. A special thanks to Mr. Anirban and all the staffs of CIF, IIT (BHU) for extending timely support for experimentation. My sincere thanks to Mr. J P Patel, Mr. Arun Prakash, Mr. Kamala Prasad, Mr. Chotey Lal, Mr. Ramji and Mr. Anjani and all the non-teaching staffs of department. I thankfully acknowledge help of my seniors Drs. Manish, Vikas Shivam, Deepa, Rajbhadrur, Arun, Vaibhav, Dhananjay, Mr. Vivek, Ms. Nandini and my fellow colleagues Ankitendran, Ankit, Avnish, Harsh, Rajat, Sakshi, Ketan, Suryaprakash, Roopchand, Saarika, Soham, Debabrata, Priyatosh and Saptarshi.

A special thanks to my family. Words cannot express their sacrifices they have made for me. Their support, moral and spiritual guidance has helped me overcoming difficult situations. Last but not the least, I am thankful to all those who have helped me throughout this period, but unwillingly I could not mention them.

Yagnesh Shadangi

TABLE OF CONTENTS

List of Figures.....	vii
List of Tables.....	xiii
Abbreviations.....	xv
Symbols.....	xvii
Preface.....	xix
Chapter 1: Introduction and Literature Review.....	1
1.1 Historical sketch.....	1
1.2 Quasicrystalline materials.....	2
1.3 Crystallography of quasicrystals.....	4
1.3.1 Penrose tiling.....	7
1.3.2 Quasi – unit cell theory.....	7
1.4 Al-Cu-Fe quasicrystals.....	8
1.4.1 Synthesis of Al-Cu-Fe quasicrystals.....	13
1.4.1.1 Rapid solidification.....	14
1.4.1.2 Mechanical alloying.....	15
1.4.1.3 Hot pressing and spark plasma sintering.....	16
1.4.1.4 Coatings of Al-Cu-Fe quasicrystals.....	16
1.5 Properties of quasicrystals.....	17
1.5.1 Physical properties.....	17
1.5.2 Surface characteristics.....	19
1.5.3 Mechanical properties.....	20
1.6 Application of quasicrystals.....	21
1.6.1 Light absorption and sensors.....	21
1.6.2 Thermal barrier coatings.....	21
1.6.3 Catalyst and hydrogen storage.....	21
1.6.4 Strengthening of alloys.....	22
1.7 High entropy alloys.....	22
1.8 Aluminium based metal matrix composites.....	24
1.8.1 AMCs reinforced with quasicrystals.....	27
1.8.2 AMCs reinforced with high-entropy alloys.....	38
1.9 Powder Metallurgy.....	41

1.9.1	Powder production	41
1.9.2	Ball milling.....	43
1.9.3	Powder consolidation	43
1.10	Motivation.....	45
1.11	Objective of the thesis.....	46
 Chapter 2: Materials and Experimental Details.....		49
2.1	Materials designation	50
2.2	Materials synthesis.....	51
2.2.1	Vacuum induction melting	51
2.2.2	Gas atomized Al alloy	52
2.3	Composite powder production.....	53
2.3.1	Vibratory ball milling.....	54
2.3.2	High energy ball milling	56
2.4	Powder compaction.....	57
2.4.1	Spark plasma sintering	57
2.4.2	Hot pressing.....	58
2.5	Structural Characterization	59
2.5.1	X-ray diffraction.....	59
2.5.2	Optical microscopy	61
2.5.3	Scanning electron microscopy	62
2.5.4	Transmission electron microscopy.....	62
2.6	Thermal stability	63
2.6.1	Differential scanning calorimetry.....	63
2.6.2	Annealing treatment	64
2.7	Physical and mechanical properties	64
2.7.1	Density measurements.....	64
2.7.2	Hardness	65
2.7.3	Compressive testing	66
 Chapter 3: Al-Cu-Fe Quasicrystalline Matrix Composite Reinforced with Sn.....		67
3.1	Structural transformation of IQC-Sn milled powder	68
3.1.1	XRD analysis of IQC-Sn milled powder.....	69

3.1.2	TEM investigation of IQC-Sn milled powder.....	82
3.2	Morphology of IQC–Sn milled powder.....	90
3.3	Thermal stability of IQC–Sn milled powder	92
3.4	Indentation behavior of IQC–Sn milled powder.....	101
3.5	Microstructure and mechanical properties of IQC–Sn bulk composite.....	105
3.5.1	IQC-Sn composite consolidated by SPS	105
3.5.2	IQC-Sn composite consolidated by hot pressing	110
3.6	Discussion.....	112
3.6.1	Structural transformation during mechanical milling	113
3.6.2	Theoretical estimation of grain size during mechanical milling.....	116
3.6.3	Thermal stability of IQC–Sn milled powder.....	119
3.6.4	Toughening behavior of IQC-Sn composite	120
3.7	Conclusions.....	121
Chapter 4: AA 6082 Al-alloy based Metal Matrix Composite Reinforced with Al-Cu-Fe Quasicrystal.....		
125		
4.1	Phase analysis of mechanically milled Al–IQC nanocomposite powder	126
4.1.2	XRD analysis of Al-IQC nanocomposite powder.....	126
4.1.2	TEM investigation of Al-IQC nanocomposite powder	136
4.2	Morphology of Al-IQC nanocomposite powder.....	141
4.3	Spark plasma sintering of Al-IQC composite.....	144
4.4	Discussion.....	154
4.4.1	Structural and microstructural features of Al-IQC milled powder	154
4.4.2	Mechanical property and interfacial strengthening of composite	157
4.5	Conclusions.....	160
Chapter 5: AA 6082 Al-alloy based Metal Matrix Composite Reinforced with Non-equiatomc AlSiCrMnFeNiCu HEA.....		
163		
5.1	Phase analysis of non–equiatomc AlSiCrMnFeNiCu HEA	164
5.1.1	XRD analysis of HEA	164
5.1.2	TEM investigation of HEA	171
5.2	Microstructure and morphology of HEA.....	174
5.3	Phase analysis of AMCs reinforced with HEA.....	178
5.3.1	XRD of Al-HEA nanocomposite powder	180

5.3.2	TEM investigation of Al-HEA milled powder.....	184
5.4	Morphology of Al-HEA milled powder	187
5.5	Thermal stability of Al-HEA milled powder	188
5.6	Pressure-less sintering of Al-HEA composite	189
5.7	Discussion.....	193
5.7.1	Phase evolution in HEA	193
5.7.2	Microstructural features and mechanical properties of Al-HEA composite	197
5.8	Conclusions.....	201
 Chapter 6: Summary and Suggestions for future work.....		203
6.1	Summary	203
6.1.1	Al-Cu-Fe quasicrystalline matrix composite reinforced with Sn.....	203
6.1.2	Al-based metal matrix composite reinforced with Al-Cu-Fe quasicrystals	205
6.1.3	Al-based metal matrix composite reinforced with AlSiCrMnFeNiCu HEA	207
6.2	Suggestions for future work.....	208
 References.....		211
List of Publications.....		239
List of Conferences Attended.....		241

LIST OF FIGURES

Figure 1. 1: (a) Bright-field image; selected area diffraction (SAD) pattern along (b) five-fold (c) three-fold [75] (d) two-fold axis of rotation in Al-Cu-Fe quasicrystal [76].	9
Figure 1. 2: (a) Equilibrium phase diagram depicting the presence of icosahedral and other crystalline phases; (b) pseudo-binary Al-Cu-Fe phase diagram for Al-Cu-Fe IQC showing phases between ω -phase ($\text{Al}_{70}\text{Cu}_{20}\text{Fe}_{10}$) and $\text{Al}_{58}\text{Cu}_{28}\text{Fe}_{14}$ [84]; (c) TTT curve as a function of temperature for Al-Cu-Fe alloy [85]; (d) compositional range for the formation of IQC phases in Al-Cu-Fe alloy by the high cooling rate [15].	12
Figure 1. 3: (a) Temperature dependence of Al-Cu-Fe and Al-Cu-Ru quasicrystals [160]; (b) Co-efficient of friction observed for Al-based ternary quasicrystals during sliding scratch test [163]; (c) True stress-strain curve of Al-Cu-Fe IQC as a function of temperature [163]; (d) Vickers microhardness of Al-Cu-Fe IQC alloy as a function of temperature [164].	18
Figure 1. 4: Evolution and stability of phases at the interfaces of Al-IQC composite during hot pressing [298].	30
Figure 2. 1: Schematic of KC-0 cryobox/vial used for fragmentation of as-cast alloys...55	
Figure 2. 2: Williamson – Hall plot for computing crystallite size and lattice strain.	60
Figure 2. 3: Precision lattice parameter by Bradley – Jay method.	61
Figure 3. 1: Phase analysis of (a) as-cast and annealed $\text{Al}_{62.5}\text{Cu}_{25}\text{Fe}_{12.5}$ (at %) IQC alloy and (b) as-received Sn powder; SEM micrograph of as-cast and annealed $\text{Al}_{62.5}\text{Cu}_{25}\text{Fe}_{12.5}$ (at %) IQC alloy and (d) as-received Sn powder.	69
Figure 3. 2: Phase transformation during MM of IQC-10Sn (a); Changes in the superlattice (311111) peak in FCI quasicrystal during MM in IQC-10Sn (b); Structural transformation of IQC to crystalline phases (c).	70
Figure 3. 3: Phase transformation during MM of IQC-20Sn (a); Changes in the superlattice (311111) peak in FCI quasicrystal during MM in IQC-20Sn (b); Structural transformation of IQC to crystalline phases (c).	72
Figure 3. 4: Phase transformation during MM of IQC-30Sn (a); Changes in the superlattice (311111) peak in FCI quasicrystal during MM in IQC-30Sn (b); Structural transformation of IQC to crystalline phases (c).	73
Figure 3. 5: Deconvolution of IQC-10Sn nanocomposite powder during MM showing the existence of IQC, Sn, and crystalline phase.....	74
Figure 3. 6: Variation of crystallite size and lattice strain of icosahedral quasicrystal and crystalline phases i.e. $\text{Al}_{13}\text{Fe}_4$ and B2-type Al(Cu, Fe) as a function of milling time in IQC-	

10Sn (a), IQC-20Sn (b), IQC-30Sn (c); Variation of crystallite size and lattice strain of Sn reinforcement in IQC-10Sn (d), IQC-20Sn (e) and IQC-30Sn (f) as a function of milling time respectively. 75

Figure 3. 7: Diffraction contrast images of IQC-10 Sn (a-c), IQC-20Sn (d-f) and IQC-30Sn (g-i); Bright field image of IQC matrix MM for 40h in IQC-10Sn (a), IQC-20Sn (d) and IQC-30Sn (g); Selected area diffraction pattern of IQC-10Sn (b), IQC-20Sn (e) and IQC-30Sn (h) corresponding to BF as shown in (a), (d) and (g) respectively; Darkfield images of IQC matrix MM for 40h in IQC-10Sn (c), IQC-20Sn (f) and IQC-30Sn (i)..... 77

Figure 3. 8: Diffraction contrast images of IQC – Sn nanocomposite showing the rod like Sn particles; (a), (d), and (g) bright-field image of Sn particle in IQC-10Sn, IQC-20Sn and IQC-30Sn respectively; (b), (e), and (h) SADP corresponding to BF image of Sn in IQC-10Sn, IQC-20Sn, IQC-30Sn respectively; (c), (f), and (i) dark-field image of Sn particles in IQC-10Sn, IQC-20Sn, and IQC-30Sn respectively. 79

Figure 3. 9: Phase contrast images of IQC-30Sn nanocomposite powder showing the presence of nanocrystalline B2-type phases (a & b) and co-existence of B2-type phase with Al₁₃Fe₄ phase (c & d)..... 80

Figure 3. 10: STEM – EDS mapping of IQC – 30Sn nanocomposite powder. 81

Figure 3. 11: SEM micrograph of IQC-10Sn (a, d), IQC-20Sn (b, e), and IQC-30Sn (c, f). 84

Figure 3. 12: Particle size distribution of IQC matrix MM for 40 h (a) IQC-10Sn, (b) IQC-20Sn, (c) IQC-30Sn; Grain size distribution of IQC matrix MM for 40 h in (d) IQC-10Sn, (e) IQC-20Sn, (f) IQC-30Sn. 85

Figure 3. 13: SEM-EDS mapping of IQC – 30Sn nanocomposite powder (a); Point EDS analysis, nominal composition, and the EDS spectrum of IQC – 30Sn (b)..... 87

Figure 3. 14: Dynamic differential scanning calorimetry thermogram of IQC-10Sn (a), IQC-20Sn (b) and IQC-30Sn (c) at a heating rate of 20 K/min, 30 K/min, 40 K/min and 50 K/min. 92

Figure 3. 15: Phase evolution during annealing of IQC-30Sn 40 h MM powder in the temperature range of 300°C to 800°C for 10h (a); Blown-up image showing phase evolution of approximant phases of IQC during annealing of IQC-30Sn 40 h MM powder in the temperature range of 300°C to 800°C for 10h (b)..... 93

Figure 3. 16: Diffraction contrast images and nano-beam diffraction (NBD) of IQC-30 Sn MM for 40h followed by annealing at 800 °C for 10h (a-c) and (d-f) respectively. Bright-field image of annealed IQC-30Sn (a); selected area diffraction pattern of annealed IQC-30Sn (b); Dark field images of annealed IQC-30Sn (c). NBD is showing (d) Al₁₃Fe₄ phase, (e) B2-type Al(Cu, Fe) phase and (f) pseudo-five fold (5-f) axis of symmetry..... 94

Figure 3. 17: SEM micrograph of IQC-30Sn MM for 40 h followed by annealing treatment at 800 °C for 10 h. The distribution of IQC phases along with Sn particles and approximant phases (a); IQC phase along with crystalline phases at higher magnification (b); EDS spectrum of point-1 (marked in blue) in Figure 3.17 (a) representing composition near to IQC phase (c); EDS spectrum of point-3 (marked in green) in Figure 3.17 (a) representing existence of rod-like Sn particle (d).....	97
Figure 3. 18: Microhardness (at an indentation load of 10 g) of IQC – Sn nanocomposite powders as a function of the duration of mechanical milling.....	99
Figure 3. 19: Load versus depth of indentation plot for IQC-10Sn (a), IQC-20Sn (b) and IQC-30Sn (c) as a function of milling duration; Variation of Hardness with milling time for IQC-10, 20 & 30Sn (d).	100
Figure 3. 20: Optical micrograph showing indentation mark on the IQC – 10Sn (a, b), IQC – 20Sn (c, d), and IQC – 30 Sn nanocomposite powder MM for 20 h and 40 h (e, f). ...	101
Figure 3. 21: Phase analysis of IQC – Sn composite SPSed at 800 °C (1073 K).....	103
Figure 3. 22: SEM micrograph of (a, d) IQC – 10Sn, (b, e) IQC – 20Sn, (c, f) IQC – 30Sn bulk composite SPSed at 800 °C (1073 K) at different magnification.	104
Figure 3. 23: Compressive stress-strain plot for (a) IQC – 10Sn, (b) IQC – 20Sn, (c) IQC – 30Sn bulk SPSed composite.	106
Figure 3. 24: Hardness value of (a) hot-pressed and (b) pressure-less sintered IQC-Sn bulk composite at different indentation loads.	108
Figure 3. 25: Optical micrograph showing indentation marks on as-cast and annealed IQC at a load of (a) 200 g and (b, c) 500 g.	109
Figure 3. 26: Optical micrograph showing indentation cracks in IQC – 10Sn hot-pressed composite; (a) sintered at 650 °C (923 K) (b) sintered at 650 °C (923 K) and (c & d) hot-pressed and annealed at 800 °C (1023 K).	109
Figure 4. 1: Phase analysis of 6082 Al alloy (a) and as-cast and annealed Al-Cu-Fe IQC alloys (b).	127
Figure 4. 2: SEM micrograph showing the morphology (a) of as received 6082 Al alloy and (b) as-cast & annealed Al-Cu-Fe IQC alloys; (c) EDS spectrum showing the chemical composition of as-cast and annealed Al-Cu-Fe IQC alloy.	128
Figure 4. 3: X-ray diffraction pattern of AA 6082 Al alloy milled for various time duration.	129
Figure 4. 4: X-ray diffraction pattern of Al-30IQC composite milled for various time duration.	130

Figure 4. 5: Phase analysis of Al-40IQC NC powder MM upto 50h (a); Structural transformation of IQC phase and approximant phases in Al-40IQC NC powder MM upto 50 h (b).....	131
Figure 4. 6: Variation of crystallite size and lattice strain of (a) Al-0IQC, (b) Al-10IQC, (c) Al-20IQC, (d) Al-30IQC, (e) Al-40IQC nanocomposite powder after mechanical milling for various duration of time.....	132
Figure 4. 7: Diffraction contrast images of Al-0IQC and Al-40IQC NC powder MM upto 50 h. Bright-field image of (a) Al-0IQC and (d) Al-40IQC NC powder; the SAD pattern of (b) Al-0IQC and (e) Al-40IQC NC powder; Darkfield image of (c) Al-0IQC and (f) Al-40IQC NC powder.....	133
Figure 4. 8: Representative TEM image (a), corresponding SAD pattern (b), HRTEM image (c) and (d) magnified HRTEM image of Al-40IQC NC powder MM upto 50 h..	134
Figure 4. 9: HAADF-STEM-EDS elemental map and corresponding EDS spectrum showing the distribution of Al, Cu and Fe in Al-40IQC NC powder MM upto 50 h.....	135
Figure 4. 10: SEM micrograph showing the morphology and nanostructured grains in (a, e) Al-0IQC, (b, f) Al-10IQC, (c, g) Al-20IQC, (d, h) Al-30IQC nanocomposite powder MM for 50 h.....	137
Figure 4. 11: Grain size distribution of (a) Al-0IQC, (b) Al-10IQC, (c) Al-20IQC, (d) Al-30IQC nanocomposite powder mechanically milled for 50 h.	138
Figure 4. 12: (a and b) Morphology and particle size distribution of Al-40IQC MM for 50 h respectively; (c) variation of particle size w.r.t volume fraction of reinforcement; (d) variation of particle size w.r.t milling duration in Al-40IQC NC powder.....	139
Figure 4. 13: Phase analysis of Al-40IQC NC powder SPSed at (a) 450 °C and (b) 550 °C; Diffraction contrast image showing (c) Bright field and (d) SAD pattern of Al-40IQC composite SPSed at 550 °C.....	140
Figure 4. 14: Back-scattered SEM micrograph showing the distribution of Al matrix and reinforcement particles at different magnification for Al-40IQC NC powder SPSed at 450 °C (a & b) and 550 °C (c & d).	142
Figure 4. 15: SEM-EDS elemental map showing the distribution of Al, Fe, Cu, Mg and Si in Al-40IQC composite SPSed at 450 °C at the interface of matrix and reinforcement..	144
Figure 4. 16: SEM-EDS elemental map showing the distribution of Al, Fe, Cu, Mg and Si in Al-40IQC composite SPSed at 550 °C at the interface of matrix and reinforcement..	145
Figure 4. 17: Phase analysis of Al-30IQC SPSed at 300 °C (573 K) with a pressure of 500 MPa; (b) enlarged view showing the co-existence of Al, IQC and crystalline phases....	146

Figure 4. 18: BSE-SEM micrograph of Al-30IQC SPSeD at 300 °C (573 K) with a pressure of 500 MPa.....	147
Figure 4. 19: Engineering compressive stress – strain diagram of Al-40IQC SPSeD at 550 °C (823 K).....	147
Figure 4. 20: Engineering compressive stress – strain diagram of (a) Al-0IQC, (b) Al-10IQC, (c) Al-20IQC, (d) Al-30IQC composite SPSeD at 300 °C (573 K) with a pressure of 500 MPa.....	148
Figure 4. 21: Fractography of (a, b, c) Al-0IQC, (d, e, f) Al-10IQC, (g, h, i) Al-20IQC, (j, k, l) Al-30IQC SPSeD at 300 °C (573 K) with a pressure of 500 MPa.....	149
Figure 5. 1: XRD pattern of (a) as-cast and (b) powdered non-equiatomic HEA.	165
Figure 5. 2: Enlarged and de-convoluted XRD pattern showing the co-existence of B2-type phase and Cr ₅ Si ₃ phase in (a, b) as-cast HEA and (c, d) powdered HEA, respectively.	166
Figure 5. 3: (a) Bright-field image and (b) selected area diffraction (SAD) pattern showing the powder particle corresponding to B2-type phase respectively; (c) Bright-field image and (d) SAD pattern showing the powder particle corresponding to Cr ₅ Si ₃ phase respectively.	167
Figure 5. 4: (a) SEM micrograph of as-cast HEA sample, (b) SEM micrograph showing the region of EDS point analysis. (c) SEM micrograph showing the morphology of fragmented as-cast powdered HEA sample, (d) Particle size distribution of fragmented powder HEA particles; (e) EDS spectrum of as-cast HEA.....	168
Figure 5. 5: SEM-EDS elemental mapping showing the distribution of alloying elements along with the presence of Cr, Si-rich region in as-cast HEA.	169
Figure 5. 6: SEM-EDS elemental mapping showing the distribution of alloying elements along with the presence of Cr, Si-rich region in as-cast powdered HEA.	170
Figure 5. 7: Phase analysis of (a) Al-10HEA nanocomposite powder MM up to 50 h; (b) enlarged image showing co-existence of Al, B2-type and Cr ₅ Si ₃ phase.	171
Figure 5. 8: Phase analysis of (a) Al-30HEA nanocomposite powder MM up to 50 h; (b) enlarged image showing co-existence of Al, B2-type and Cr ₅ Si ₃ phase.	172
Figure 5. 9: Variation of crystallite size and lattice strain during mechanical milling of (a) Al-10HEA, (b) Al-20HEA, (c) Al-30HEA.....	173
Figure 5. 10: TEM micrograph of Al-30HEA nanocomposite showing the (a) bright-field image (b) corresponding selected area diffraction pattern, (c) dark field image, and (d) grain size distribution in nanocomposites.	175

Figure 5. 11: SEM micrograph of Al-HEA nanocomposite powder showing morphology after 50 h of MM in Al-10HEA (a, b), Al-20HEA (c,d), and Al-30HEA at different magnification.	177
Figure 5. 12: Particle size distribution of (a) Al-10HEA (b) Al-20 HEA and (c) Al-30HEA nanocomposite powder mechanically milled up to 50 h.....	179
Figure 5. 13: DSC thermogram of (a) as-cast powdered non-equiatomic HEA; (b) Al-30HEA nanocomposite at a 20 K/min scan rate.	180
Figure 5. 14: In-situ XRD pattern ($\lambda=0.15402$ nm) of Al-30HEA at high temperatures.	181
Figure 5. 15: SEM micrograph of (a & d) Al-10HEA, (b & e) Al-20HEA, (c & f) Al-30HEA consolidated by pressure-less sintering.	184
Figure 5. 16: SEM-EDS mapping of Al-30HEA composite consolidated by pressure-less sintering.....	185
Figure 5. 17: Load versus indentation depth plot for (a) Al-10HEA (b) Al-20HEA and (c) Al-30HEA composite; (d) variation of hardness and depth of indentation as a function of volume fraction of HEA reinforcement in Al-HEA pressure-less sintered composite....	186
Figure 5. 18: Property diagram for non-equiatomic AlSiCrMnFeNiCu HEA by ThermoCalc.....	192

LIST OF TABLES

Table 1. 1: Important binary and ternary phases in Al-Cu-Fe alloy system [60].	10
Table 1. 2: Non-equilibrium processing routes for the synthesis of quasicrystals [60]... 13	
Table 1. 3: Mechanical properties of AMCs reinforced with Al-based quasicrystals.	31
Table 1. 4: Mechanical properties of AMCs reinforced with HEA particulates processed through various techniques.	39
Table 2. 1: Designation of composite synthesized in the present investigation.	50
Table 2. 2: Physical properties of elements used for the synthesis of alloys and composites.	51
Table 2. 3: Chemical composition of gas atomized 6082 Al alloy powder used for AMCs.	53
Table 2. 4: Weight fraction of matrix and reinforcement used for the synthesis of nanocomposites.	54
Table 2. 5: Protocol for mechanical milling of nanocomposite powders.	56
Table 2. 6: Processing parameters of IQC-Sn and Al-IQC composites during SPS.....	58
Table 3. 1: Variation of Crystallite size and lattice strain in IQC-Sn nanocomposites. ..	76
Table 3. 2: Variation of particle size and grain size in IQC-Sn nanocomposite powder.	90
Table 3. 3: Chemical composition of IQC-Sn nanocomposite powder derived from SEM-EDS.	91
Table 3. 4: Activation energy calculation for phase evolution during heating of IQC-Sn milled powder.	96
Table 3. 5: Chemical composition of corresponding to point-1, 2, and 3 as marked in Figure 3.17 (a) with blue, green, and red circles, respectively.	98
Table 3. 6: The hardness of IQC-Sn milled powder.	102
Table 3. 7: Physical and mechanical properties of IQC – Sn bulk SPSed composite. ..	107
Table 3. 8: Fracture toughness of IQC–Sn hot-pressed composite.....	112
Table 3. 9: Parameters for estimating minimum grain/crystallite size during MM.	118

Table 4. 1: Crystallite size and lattice strain during mechanical milling of Al – IQC nanocomposite powder.	131
Table 4. 2: Elemental composition of phases in Al-40IQC composite SPSed at 450 °C (723 K) and 550 °C (823 K).	143
Table 4. 3: Physical and mechanical property of SPSed Al-40IQC matrix composite. .	151
Table 4. 4: Physical and mechanical property of Al-IQC matrix composite SPSed at 300 °C (573 K) with a pressure of 500 MPa.	152
Table 5. 1: Crystallite size, lattice strain, and dislocation density of the Al-HEA nanocomposite powder as a function of milling duration and volume fraction of reinforcement.	174
Table 5. 2: Elemental composition of as – cast non-equiatomic AlSiCrMnFeNiCu HEA.	176
Table 5. 3: Hardness of Al-HEA pressure-less sintered composite.	187
Table 5. 4: Chemical enthalpy of mixing ($\Delta H^{\text{mix}}_{ij}$, kJ/mol) of atomic pairs for non-equiatomic AlSiCrMnFeNiCu HEA alloy following the Miedema's approach [404–406].	190
Table 5. 5: Calculate thermodynamic and physical parameter of non-equiatomic AlSiCrMnFeNiCu HEA.	190
Table 5. 6: Physical properties of alloying elements in non-equiatomic HEA.	197

ABBREVIATIONS

QC	Quasicrystal
HEA	High Entropy Alloy
MMC	Metal Matrix Composite
AMC	Aluminium Matrix Composite
IQC	Icosahedral Quasicrystal
NC	Nanocomposite
HP	Hot Pressing
VHP	Vacuum Hot Pressing
CP	Cold Pressing
CIP	Cold Isostatic Pressing
BCC	Body Centered Cubic
OM	Optical Microscopy
DSC	Differential Scanning Calorimeter
EDS/EDX	Energy Dispersive X- ray Spectroscopy
FCC	Face Centered Cubic
FSP	Friction Stir Processing
SFSP	Submerged Friction Stir Processing
HADDF	High Angle Annular Dark Field
HIP	Hot Isostatic Pressing
HE	Hot Extrusion
HRTEM	High Resolution Transmission Electron Microscopy
MA	Mechanical Alloying
MM	Mechanical Milling
HEM	High Energy Ball Milling
HT	Heat Treatment
PCA	Process Control Agent
SEM	Scanning Electron Microscopy
SLM	Selective Laser Melting
SPS	Spark Plasma Sintering

STEM	Scanning Transmission Electron Microscopy
TEM	Transmission Electron Microscopy
VEC	Valence Electron Concentration
VIM	Vacuum Induction Melting
VAM	Vacuum Arc Melting
XRD	X-Ray Diffraction

SYMBOLS

A	Lattice Parameter
β	Beta
$^{\circ}\text{C}$	Degree Centigrade
K	Kelvin
N	Newton
Pa	Pascal
MPa	Megapascal
GPa	Gigapascal
θ	Theta
Ψ	Chi
δ	Delta
Ω	Omega
m	Meter
μm	Micrometer (micron)
nm	Nanometer
at%	Atomic Percent
wt%	Weight Percent
mm	Millimeter
g	Gram
l	Litre
ml	Millitre
J	Joule
cm	Centimeter
h	Hour
min	Minute
s	Second
R	Ideal Gas Constant
<	Less than
>	Greater than

σ

Å

λ

HV

Sigma

Angstrom

Wavelength

Vickers Hardness

PREFACE

The surge for the design and development for new and advanced materials have always been enticing to the materials engineering & science community. The intermetallics and metal matrix composites (MMCs) are receiving increasing attention among the advanced materials due to their high strength, stiffness and high-temperature properties. The intermetallic compounds have emerged as technologically important materials widely used for high-temperature applications. The discovery of aperiodic intermetallics i.e., quasicrystals in 1984 by Dan Shechtman has been a path-breaking development, which has redefined the conventional concept of crystallography. The inherent room temperature brittleness and reduced dislocation activity of periodic and aperiodic intermetallics have resulted in its low fracture toughness. This low values of fracture toughness often restrict its large scale structural applications. Similarly, in the year 2004, yet another paradigm shift in the materials development strategy has given birth to the concept of high-entropy alloys (HEAs) having five or more than five alloying elements in equiatomic, near equiatomic or non-equiatomic ratio. These HEAs was first reported by Brian Cantor and J W Yeh independently and despite having five or more elements in equiatomic proportions mostly resulted in disordered solid solution. On the other hand, the aluminium matrix composites (AMCs) falling under the class of MMCs have received much attention due to their high strength to weight ratio. Designing and finding suitable reinforcement for these AMCs has always been challenging as well as awarding. For developing high strength AMCs, Al-based metal matrices have been reinforced with quasicrystals and HEAs.

The processing of these advanced materials is equally necessary for developing materials for engineering applications. The nanostructured alloys and AMCs have better properties compared to their conventional counterpart. The nanostructuring of the aperiodic

intermetallics (i.e. quasicrystals) and AMCs improves its strength and toughness. These nanostructures alloys and AMCs can be synthesized by solid-state techniques, i.e. mechanical milling. Non-equilibrium processing routes can synthesize the nanostructured alloys and AMCs for tailoring their physical and mechanical properties. The consolidation of these nanostructured alloys and AMCs are challenging and can be accomplished through various non-equilibrium consolidation techniques like spark plasma sintering (SPS), vacuum hot-pressing (VHP), and hot isostatic pressing (HIP).

The present work deals with the synthesis and processing of the nanocomposites of Al-Cu-Fe quasicrystalline matrix reinforced with Sn particles and AA 6082 Al matrix reinforced with Al-Cu-Fe icosahedral quasicrystal (IQC) and non-equiatomic AlSiCrMnFeNiCu HEA. The study aims at understanding the structural transformation, thermal stability and microstructural features of these nanocomposite powders. Attempts were made to consolidate these nanocomposite powders through SPS, hot-pressing (HP) and pressure-less sintering. The structure, microstructure and mechanical properties of these bulk composites were studied in detail.

The thesis is divided into six chapters. **Chapter-1** presents the introduction and current understanding of the theme of the work based on the reviewed literature available. This chapter briefly describes the timeline for design and development of the new materials, i.e. quasicrystals, high-entropy alloy and high strength Al matrix composites. The crystallography, properties and applications of quasicrystals was described along with present shortcomings for its application as a structural material. The section on the AMCs briefly discusses the AMCs reinforced with various unconventional reinforcement such as quasicrystals and HEAs. This chapter also concerns the different material processing

methodology being used in the present work. The objectives of the present study are listed at the end of this chapter.

Chapter-2 describes the details of the materials and experimental procedure used for the present work. This chapter mentions the equipment and protocol required for materials processing and its characterization. Vacuum induction melting was used for preparing as-cast quasicrystalline and non-equiatomic high-entropy alloy (HEA) and was further crushed into a particle size of $\leq 100 \mu\text{m}$. Mechanical milling (MM) was used for synthesis nanocomposite powders of quasicrystalline and Al matrix composite through high energy planetary ball milling. The structural and microstructural features of these nanocomposites were studied through X-ray diffraction (XRD) and transmission electron microscopy (TEM), and scanning electron microscopy (SEM) equipped with energy dispersive spectroscopy. The thermal stability of these nanocomposite powders was established through differential scanning calorimetry (DSC). The heating events in the DSC thermogram were co-related with the phases evolved by ex-situ XRD of annealed composite powder or by in-situ XRD. The hardness and indentation behaviour of these nanocomposite powders studied through microindentation and nanoindentation techniques. Further, these nanocomposite powders were consolidated through SPS, HP and pressure-less sintering for fabricating bulk composite. The phase analysis and microstructure of bulk composites were studied through XRD and TEM, and optical microscopy (OM) and SEM, respectively. The mechanical properties of these bulk composites were investigated through microhardness and compressive testing.

Chapter-3 presents the investigation on the mechanically driven structural transformation in Sn reinforced Al-Cu-Fe quasicrystalline (IQC) matrix nanocomposite (NC). The sequence of structural transformation, phase composition, thermal stability and hardness of

mechanically milled IQC-Sn NC powder were studied. The XRD result suggests the formation of nanostructured composites. The IQC phase co-existed with $Al_{13}Fe_4$ ($a=1.549$ nm, $b=0.808$ nm, $c=1.248$ nm, $\alpha=\beta=90^\circ$, $\gamma=107.720^\circ$; mC102; C2/m) and B2-type Al (Cu, Fe) ($a=0.29$ nm; cP2; $Pm\bar{3}m$) phase, in IQC-Sn NC powder subjected to MM for 40 h. The double diffraction was observed due to the layering of nanocrystalline B2 and IQC phase in the NC powder. The inner concentric and outer ring corresponds to the B2-type and (422222) reflection of the IQC phase, respectively. The phases formed during MM transforms to stable IQC phase along with crystalline phases during subsequent annealing treatment as confirmed by XRD and nano-beam diffraction (NBD). The structural transformations occurring during MM have a remarkable effect on indentation hardness, which is in the range of ~ 4 to 7 GPa. This nanocomposite powder was consolidated by SPS, HP, and pressure-less sintering. The phase evolved in SPSed IQC-Sn composite was also found to be dependent on the volume fraction of Sn reinforcement in the IQC matrix. The bulk composite prepared by SPS has shown significant enhancement in the compressive yield strength $\sim 75\%$ for IQC-20Sn. The fracture toughness of the IQC-10Sn HPed composite was found to increase by $\sim 22\%$. The increase in the compressive yield strength and fracture toughness of these bulk composite was attributed to the inhibition of cracks by soft Sn particles homogeneously dispersed in the IQC matrix by milling and sintering.

Chapter-4 deals with studying the effect of Al-Cu-Fe IQC reinforcement on the structure, morphology and phase composition of AA 6082 Al matrix nanocomposites processed through mechanical milling and SPS. The characterization of these milled and SPSed AMCs was done through XRD, TEM, and SEM. The MM induces microstructural refinement of the matrix, and the extent of improvement was dependent on the volume fraction of the IQC. However, the partial structural transformation of IQC phase to $Al_{13}Fe_4$

crystalline phase ($a=1.549$ nm, $b=0.808$ nm, $c=1.248$ nm, $\alpha=\beta=90^\circ$, $\gamma=107.720^\circ$; $mC102$; $C2/m$) was only evident for AMCs reinforced with 40 vol% of IQC. The presence of (311111) diffraction peak of the IQC phase in AMCs confirms the existence of face-centred IQC phase even after 50 h of MM. The Al-IQC was consolidated at 300 °C (573 K) with a pressure of 500 MPa, and another set of the sample was consolidated at 450 °C (723 K) and 550 °C (823 K) with a pressure of 50 MPa. It was observed that on increasing the reinforcement in AMCs, the relative density of the composite increases and reaches a maximum value of 99.5% for Al-40IQC. The compressive yield strength and ultimate strength of these AMCs is ~519 MPa and 639 MPa respectively. However, the Al-30IQC SPSed at 300 °C (573 K) with a pressure of 500 MPa for 30 min has resulted in a significant rise in the compressive yield strength ~900 MPa. The enhancement in the mechanical properties may be attributed to strong interfacial bonding of the Al matrix and IQC reinforcement due to interfacial reactions.

Chapter-5 concerns with investigating the effect of non-equiatomic AlSiCrMnFeNiCu high-entropy alloy (HEA) reinforced Al-based metal matrix composite. These HEA used as reinforcement was prepared by vacuum induction melting followed by 30 min milling for its fragmentation. The HEA was reinforced into the AA 6082 Al matrix by MM followed by pressure-less sintering. The structure, microstructure and morphology, compositional analysis, and thermal stability of these HEA and Al-HEA nanocomposite powders were ascertained using XRD and TEM, SEM-EDS, and DSC respectively. The HEA used as reinforcement was found to have a two-phase microstructure with a major phase corresponding to the B2-type and a minor phase of Cr_5Si_3 . The MM imparts significant refinement of the Al matrix, and a nanostructured grain of ~10-12 nm was observed for Al-30HEA nanocomposite powder. For AMCs with a higher fraction of reinforcement, the HEA was found to be well embedded in the 6082 Al matrix and has an

excellent interfacial bonding. The Al-30HEA nanocomposite powder was found to be thermally stable up to 650 °C (923 K). This was confirmed by correlating the DSC thermogram with the in-situ XRD investigations. It provided a basis for the consolidation of Al-HEA composite at high temperature through pressure-less sintering. The pressure-less sintering of Al-30HEA has led to the formation of a thin ~500 nm transitional layer at the interface of 6082 Al matrix and HEA reinforcement. The microhardness of Al-HEA composite was found to be encouraging, and a maximum microhardness of ~1.72 GPa was observed for Al-30HEA composite. This high value of microhardness was attributed due to the formation of the transitional layer and indirect strengthening of Al-HEA composite.

Chapter-6 presents a summary of the work indicating major findings and observation arising out from the present work along with the suggestions for future work.

Reference section provides the list of relevant references (~400) cited in Chapter 1-6 of the thesis.